J. Math. Biol. (2013) 66:1475–1497
DOI 10.1007/s00285-012-0541-x

Mathematical Biology

Neural field theory with variance dynamics

P. A. Robinson

Received: 26 May 2011 / Revised: 15 April 2012 / Published online: 11 May 2012

Abstract Previous neural field models have mostly been concerned with prediction of mean neural activity and with second order quantities such as its variance, but without feedback of second order quantities on the dynamics. Here the effects of feedback of the variance on the steady states and adiabatic dynamics of neural systems are calculated using linear neural field theory to estimate the neural voltage variance, then including this quantity in the total variance parameter of the nonlinear firing rate-voltage response function, and thus into determination of the fixed points and the variance itself. The general results further clarify the limits of validity of approaches with and without inclusion of variance dynamics. Specific applications show that stability against a saddle-node bifurcation is reduced in a purely cortical system, but can be either increased or decreased in the corticothalamic case, depending on the initial state. Estimates of critical variance scalings near saddle-node bifurcation are also found, including physiologically based normalizations and new scalings for mean firing rate and the position of the bifurcation.

Keywords Neural field theory · Networks · Brain dynamics

Mathematics Subject Classification 92C42 · 92C20 · 92B25 · 92C05

P. A. Robinson (✉)
School of Physics, University of Sydney, Sydney, NSW 2006, Australia
e-mail: robinson@physics.usyd.edu.au

P. A. Robinson
Brain Dynamics Center, Sydney Medical School, Western, University of Sydney, Westmead, NSW 2145, Australia

1 Introduction

Physiologically based neural-field modeling of brain activity has enabled successful predictions of a wide variety of phenomena in normal waking and sleeping brain states and abnormal regimes (Robinson et al. 1997, 1998, 2000, 2001, 2002, 2004, 2007; Robinson 2005; Rowe et al. 2004; Bressloff 2002; Bressloff and Cowan 2002; O'Connor and Robinson 2003; O'Connor et al. 2002; Rennie et al. 2002; Deco et al. 2008; Jirsa and Haken 1996; Steyn-Ross et al. 1999, 2001b,a, 2005a,b, 2006; Nunez 1995; Wright and Liley 1996; Freeman 1975; Lopes da Silva et al. 1974; Wilson et al. 1973; Breakspear et al. 2006; Kim and Robinson 2007; Nunez 1974; Suffczynski et al. 2006, 2005; Liley and Bojak 2005). These include time series, spectra, correlation and coherence functions, and other properties of electroencephalograms (EEGs), responses evoked by impulsive or sinusoidal stimuli, and links with functional magnetic resonance imaging (fMRI) via the blood oxygen level dependent (BOLD) signal. Despite the highly nonlinear nature of many neural phenomena, these works have found that a large body of experimental results in these areas can be successfully accounted for by linear dynamics relative to a nonlinearly determined fixed point of normal brain activity. However, it is also clear that many phenomena, especially seizures, require nonlinear analysis of the dynamics of neural field equations, which yield time series and bifurcation structures that are in good agreement with observations (Robinson et al. 2002; Breakspear et al. 2006; Kim and Robinson 2007).

While nonlinear analyses of a given physiological model are more general than linear ones, linear analyses typically yield much greater insight, often in analytic form, within their regimes of validity. Typically, they yield the linear dynamics of mean quantities such as firing rates and soma voltages, relative to a fixed point, which is determined from the steady-state solutions of the fully nonlinear neural field equations. Quadratic quantities, such as power spectra and correlation functions are easily computed for small perturbations from steady states, but do not affect the original steady states in such analyses. Adding feedback of such quantities on the dynamics in the vicinity of the steady state will allow the regime of validity of the linear approximation to be better understood, and will enable an expansion of the analytically tractable regime to include weak nonlinearities.

One potential mechanism for such a feedback is the effect of voltage fluctuations on the voltage diffusion of neurons from their post-spike voltage back to firing threshold, as studied in stochastic leaky integrate-and-fire neural models, for example (Meffin et al. 2004), where this diffusion rate has been shown to broaden the distribution of effective thresholds.

The firing threshold distribution enters neural field theories via parameters of the relationship assumed between firing rate and soma voltage (Freeman 1975; Robinson et al. 2007). In most neural-field theories, this is approximated by a sigmoidal function, with a transition from low to high firing rates, whose width reflects the distribution of neural properties and inputs relative to the mean. In most cases, this width is assumed to be constant, but this ignores the effects of population variance in soma voltage, or equivalently afferent spike rates, on the fraction of neurons that attain their individual firing thresholds per unit time: a larger variance in inputs means that the neurons in the broadened tail of the distribution can reach threshold and fire more often. This effect

is well known in the literature on leaky integrate-and-fire (LIF) neurons (Meffin et al. 2004), for example, but has not yet been fully explored in neural field theory, despite several recent papers on generalizing standard mean-field approximations in various models (Buice and Cowan 2007, 2009; Buice et al. 2010; Bressloff 2009; Marreiros et al. 2008, 2010); in particular, applications to critical points and critical scalings remain to be explored in detail—a particular focus of the present work.

In Sect. 2 we write down nonlinear neural field equations, including the effect of the voltage variance on the sigmoidal function by making the approximation of Gaussian-distributed voltage fluctuations. We then approximate this variance in terms of linear transfer functions that relate it to the variance of external inputs to the brain, which we approximate as spatiotemporally white. These forms diverge near certain bifurcation points (Robinson et al. 1997; Steyn-Ross et al. 1999, 2006)—saddle-node bifurcations in particular—so their linear approximations eventually break down in those neighborhoods. However, the existence of the divergence is robust and, away from the singularity, the quantitative form is also correct. The results here enable the limits of validity of approaches with and without inclusion of variance feedback to be clarified. The effects on a cortical system are explored and illustrated in Sect. 3, along with discussion of the corticothalamic case. In Sect. 4 we summarize the main results.

2 Theory

Here we write down the neural field equations of interest, based closely on those of Robinson et al. (1997) and Robinson (2005), to which papers the reader is referred for further details, especially of the physiological details and approximations made. In doing so, we generalize these equations to incorporate how the variance of neural activity affects the sigmoidal function that relates mean firing rate to soma voltage. We then estimate the variances using linear transfer functions and discuss the regime of validity of analyses with and without variance feedback.

2.1 Neural field equations

As in previous work, we make a continuum approximation in which neural properties are averaged over spatial scales of a tenth of a mm or so: sufficient to contain large numbers of neurons, but small enough to resolve quite fine structure in the brain and its activity. To focus on the effects of interest, we specialize here to the case where all parameters, other than the transition width of the sigmoidal rate-voltage response function, are treated as constant.

We assume that the brain contains multiple populations of neurons, distinguished by a subscript a, which simultaneously labels both the structure in which a given population lies (e.g., a particular nucleus) and the type of neuron (e.g., interneuron, pyramidal cell). The continuum soma potential V_a is the sum of contributions V_{ab} resulting at the soma from activity that arrives at each type of (mainly) dendritic synapse b, where b denotes both the afferent (incoming) population and neurotransmitter type. Thus we write

$$V_a(\mathbf{r},t) = \sum_b V_{ab}(\mathbf{r},t), \tag{1}$$

where $\mathbf{r}$ denotes the spatial coordinates, t the time, the summation is assumed to be linear, and all potentials are measured relative to resting. The cortex is approximated as a two dimensional sheet and $\mathbf{r}$ is assumed to be the actual position in the case of the cortex. Some key structures, such as the thalamus, are linked to the cortex via a primary topographic map (which does not exclude the possibility of other connections), that links points in a one-to-one manner between structures, so we assign the same value of $\mathbf{r}$ to such points. Hence, in structures other than the cortex, the map coordinate $\mathbf{r}$ denotes a *rescaled* physical dimension (i.e., the physical coordinate multiplied by the ratio of the cortical scale to the structure's scale), a point that must be remembered when considering values of spatial parameters in these structures.

The subpotentials V_{ab} respond in different ways to incoming spikes, depending on their synaptic dynamics (ion-channel kinetics, diffusion in the synaptic cleft, release and reuptake processes, etc.), subsequent signal dispersion in the dendrites, and capacitive effects at the cell body. The resulting response of the soma potential to a delta-function input at the synapse can be approximated via the differential equation (Robinson et al. 1997)

$$D_{ab}(\mathbf{r},t)V_{ab}(\mathbf{r},t) = \nu_{ab}(\mathbf{r},t)\phi_{ab}(\mathbf{r},t-\tau_{ab}), \tag{2}$$

$$D_{ab}(\mathbf{r},t) = \frac{1}{\alpha_{ab}\beta_{ab}}\frac{d^2}{dt^2} + \left(\frac{1}{\alpha_{ab}} + \frac{1}{\beta_{ab}}\right)\frac{d}{dt} + 1, \tag{3}$$

where α_{ab} is the mean decay rate of the soma response to a delta-function synaptic input, β_{ab} is the mean rise rate, τ_{ab} is the discrete time delay between remotely situated populations, which is assumed constant here, ν_{ab} is a local coupling-strength, given by

$$\nu_{ab} = N_{ab}s_{ab}, \tag{4}$$

where N_{ab} is the mean number of connections from cells of type b per cell of type a and s_{ab} is their mean strength, and where the pulse density field ϕ_{ab} is the weighted average rate at which spikes arrive at $(\mathbf{r},t)$ and comprises signals from population b to a.

Action potentials are produced at the axonal hillock when the soma potential exceeds a threshold θ_a. When averaged over a population of neurons with normal response characteristics, a good approximation to the firing rate Q_a is

$$Q_a(\mathbf{r},t) = Q_{a\max}S_a[V_a(\mathbf{r},t);\sigma_a], \tag{5}$$

where $Q_{a\max}$ is the maximum firing rate, S_a is the rate-voltage response function, and σ_a is the population standard deviation of the soma voltage relative to the firing threshold. We examine (5) in detail in Sect. 2.2.

Considerable theoretical and experimental work has shown that, to a good approximation, the mean field of axonal signals propagates within a smoothly structured neural population approximately as if governed by a damped wave equation (Robinson 2005; Jirsa and Haken 1996; Robinson et al. 1997; Nunez 1995; Xu et al. 2007; Rubino et al. 2006; Schiff et al. 2007). For an isotropic damped wave equation of the form (Robinson et al. 1997; Robinson 2005)

$$\left[\frac{1}{\gamma_{ab}^2}\frac{\partial^2}{\partial t^2}+\frac{2}{\gamma_{ab}}\frac{\partial}{\partial t}+1-r_{ab}^2\nabla^2\right]\phi_{ab}(\mathbf{r},t)=Q_b(\mathbf{r},t), \tag{6}$$

where $\gamma_{ab}=v_{ab}/r_{ab}$ is the temporal damping coefficient and v_{ab} is the wave velocity in coordinate units. We note that this equation is the two-dimensional generalization of the telegrapher's equation.

Equation (6) encapsulates propagation from soma location to soma location. The effective range r_{ab} of the propagator accounts for both the coordinate divergence h_{ab} of fibers traveling from b to a and the extent of arborization d_a of dendritic trees of type a, giving an approximate range $r_{ab}=(h_{ab}^2+d_a^2)^{1/2}$.

2.2 Rate-voltage response function

We now examine the population-averaged rate-voltage response function (5) in detail, in order to approximate the effects of the variance in soma voltage on its form.

A neuron produces action potentials, or spikes, when its soma potential exceeds a threshold $\tilde{\theta}_a$, where the tilde indicates the value for an individual neuron. After the spike, the potential resets to a lower value $\tilde{V}_a^{res}$. In idealized analyses, these values are the same for all neurons, but real neurons have a distribution of numbers and conductivities of ion channels, and other relevant biophysical quantities, which lead to probability distributions of both potentials; in particular, we assume here that $\tilde{\theta}$ has the Gaussian distribution

$$p(\tilde{\theta}_a;\sigma_{\theta a})=\frac{1}{\sigma_{\theta a}\sqrt{2\pi}}\exp\left[-\frac{(\tilde{\theta}_a-\theta_a)^2}{2\sigma_{\theta a}^2}\right], \tag{7}$$

where $\sigma_{\theta a}$ is the standard deviation. To focus on the effects of variance in the present work, we do not include additional complexities such as modulation of the threshold by the effects of slow currents that can lead to history-dependent bursting behavior, for example; however, these can be straightforwardly included in mean-field modeling (Robinson et al. 2007).

It is the distribution of $\tilde{V}_a-\tilde{\theta}_a$ of soma voltage relative to threshold that determines the rate at which neurons reach threshold and fire. The distributions of $\tilde{V}_a$ and $\tilde{\theta}_a$ must thus be convolved, whence the standard deviation σ_{Va} of $\tilde{V}_a$ affects the distribution that determines the firing rate. Neurons in vivo usually fire as a result of many small inputs, rather than a few large ones or a steady current, as in in vitro experiments (Deco et al. 2008). Stochasticity in the arrival rate of these inputs yields variance in the soma potential relative to threshold, which smears out the response function for a

given mean potential. Equivalently, the effective value of σ_a is increased. If we assume a Gaussian distribution as the simplest approximation, the net effect is to increase the relevant variance from $\sigma_{\theta a}$ to a value given by

$$\sigma_a^2 = \sigma_{\theta a}^2 + \sigma_{Va}^2. \tag{8}$$

Incidentally, the assumption of an approximately Gaussian form is also supported by stochastic neuron theory, which has shown that the distribution of leaky integrate and fire (LIF) neurons with a reset voltage V_a^{res} for $V_a^{res} < V_a < \theta_a$, is a Gaussian modified by a cutoff due to the absorbing boundary condition at $\tilde{\theta}_a$ that arises from the firing and consequent voltage reset that occur at that point. The effect of adding variance in the threshold is to make the distribution of voltage relative to threshold broader than that for fixed threshold, as in (8) (Marreiros et al. 2008, 2010). The Gaussian approximation captures the key qualitative effect, but could break down in detail if the input signals were significantly skewed, or if endogenous oscillations were generated by the system, e.g., as in seizures (Robinson et al. 2002; Breakspear et al. 2006).

The effective rate-voltage response function, averaged over the population can now be written in the form (5), with σ_a interpreted as in (8), whereas previous work omitted the last term in (8). A commonly used approximation to the resulting sigmoidal rate-voltage response function, written in terms of mean quantities, is

$$S_a[V_a(\mathbf{r},t);\sigma_a)] = \frac{1}{1+\exp[-C\{V_a(\mathbf{r},t)-\theta_a\}/\sigma_a]}, \tag{9}$$

where $C = \pi/\sqrt{3}$. The derivative of (9) with respect to V_a defines a probability density $\rho_a(V_a)/Q_{\max}$ of voltage relative to threshold that approximates a Gaussian (the factor $Q_{\max}$ is included to accord with notation in previous works and below). An alternative form of (9) is

$$S_a[V_a(\mathbf{r},t);\sigma_a)] = \frac{1}{2}(1+\mathrm{erf}[\{V_a(\mathbf{r},t)-\theta_a\}/\sigma_a\sqrt{2}]), \tag{10}$$

whose derivative is Gaussian with standard deviation σ_a.

2.3 Approximation of voltage variance

To close our system of equations (1)–(9), we need to calculate the voltage variance σ_{Va}^2. We note that these equations have been found to have an odd number of fixed points for constant σ_a, and we assume that at least one stable fixed point exists in the cases of interest here, as has been established previously for fixed σ_a (Robinson et al. 1998, 2004). We then expand (1)–(9) to first order relative to this fixed point and approximate the variance by its linear value; i.e., the value relative to the fixed point, whose location is now determined in part by the variance itself. As mentioned earlier, the quantitative accuracy of the approximation will break down when the variance is large enough that $\sigma_{Va} > \sigma_{\theta a}$. This is because the sigmoid (9) can be approximated by

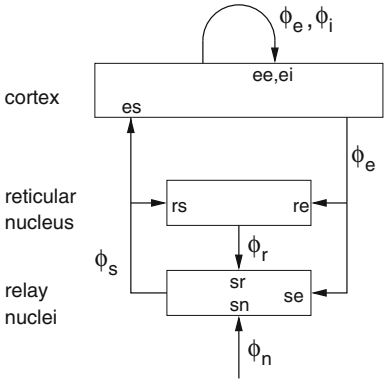

Fig. 1 Schematic of connectivities in the corticothalamic system considered. The cortical populations of excitatory (e) and inhibitory (i) neurons are shown, along with those of the reticular (r) and specific (s) relay nuclei of the thalamus. Also shown are the pulse-rate fields ϕ_{ab} ($= \phi_b$ under the random connectivity approximation, RCA), including the external input ϕ_{sn} ($= \phi_n$ under the RCA). A cortical system is obtained by deleting the reticular nucleus and the cortical feedback to the relay nuclei, making the latter part of the input pathway

a straight line only over voltage ranges smaller than the characteristic range $\sigma_{\theta a}$ over which its curvature can be neglected. Hence, the linear approximation will break down, for example, very near a saddle-node bifurcation where the fixed point loses stability and σ_{Va} becomes large; however, it is accurate in the linearly stable regime away from this point, and certainly better than the assumption of constant σ_a in previous work, which is a limiting case of the present analysis.

The corticothalamic system of interest here is shown schematically in Fig. 1, where the input ϕ_{sn} determines the other ϕ_{ab}. The V_a are then determined by (1) and (2), where the labels a are summarized in the caption. Their linear variances can be straightforwardly estimated by Fourier methods, using the transfer functions $T_{an}(\mathbf{k}, \omega) = V_a(\mathbf{k}, \omega)/V_n(\mathbf{k}, \omega)$ that link voltage fluctuations $V_a(\mathbf{k}, \omega)$ at wave vector $\mathbf{k}$ and angular frequency ω to those in the external noise source $V_n(\mathbf{k}, \omega)$ that sets the overall level of fluctuations (Robinson 2005; Robinson et al. 1997). Here, all quantities in Fourier space denote first-order perturbations relative to the assumed fixed point. We also write ϕ_{sn} and Q_n in terms of V_n, simply to enable the results to be expressed in terms of voltage transfer functions; this gives $\phi_{sn}(\mathbf{k}, \omega) = Q_n(\mathbf{k}, \omega) = \rho_n V_n(\mathbf{k}, \omega)$. This latter assumption places no special restriction on the input ϕ_{sn} received at the thalamus, which is the physically relevant quantity; nor does it involve any specific assumptions about sensory input systems.

In answer to the possible objection that many aspects of brain dynamics are nonlinear, we note that a large-scale fixed point is entirely compatible with nonlinear dynamics at the small scale (e.g., nonlinear generation of axon potentials and nonlinear interactions of microscopic neural assemblies). Moreover, there is extensive evidence that large-scale linear instabilities are associated with the onset of nonlinear dynamics involving excessive synchrony, such as during epileptic seizures (Robinson et al. 2002; Breakspear et al. 2006).

The variance of V_a can be written

$$\sigma_{Va}^2 = \sum_{\mathbf{K}} \int \frac{d\omega}{2\pi} |T_{an}(\mathbf{K}, \omega)|^2 |V_n(\mathbf{K}, \omega)|^2, \tag{11}$$

where $\mathbf{K}$ runs over the wavevectors (more generally the spatial eigenvalues) that label the spatial eigenfunctions of the system, which is of finite physical size (Robinson et al. 2000). It has been shown previously that, in the absence of large discrete stimuli, a wide variety of EEG phenomena can be quantitatively accounted for by approximating $V_n(\mathbf{K}, \omega)$ by white noise in (11) (Robinson 2005; Robinson et al. 1997, 2001; Deco et al. 2008; Steyn-Ross et al. 1999, 2006), whose modulus is assumed to be a constant U_n henceforth. We thus find

$$\sigma_{Va}^2 = U_n^2 \sum_{\mathbf{K}} \int \frac{d\omega}{2\pi} |T_{an}(\mathbf{K}, \omega)|^2. \tag{12}$$

Strictly, a low-frequency cutoff should be imposed in (12) so that fluctuations with $\omega \ll Q_a$ are treated as nonrandom; however, the result is semiquantitatively correct without this refinement, but we note that it would tend to somewhat reduce the effects found below.

Here we are chiefly concerned with the effects of variance on the global steady states about which linearization is carried out, which have $\mathbf{K} = \mathbf{0}$. Because these correspond to $\mathbf{K} = \mathbf{0}$ and the activity spectra that give rise to the variance are dominated by low K and ω, we restrict attention to $\mathbf{K} = \mathbf{0}$ in what follows, and omit the first argument of the quantities on the right of (12) when this leads to no confusion. Hence, (12) becomes

$$\sigma_{Va}^2 = U_n^2 \int \frac{d\omega}{2\pi} |T_{an}(\omega)|^2, \tag{13}$$

with $T_{an}(\omega) = T_{an}(\mathbf{0}, \omega)$. These approximations can be relaxed straightforwardly, and it is worth noting that it is a common misconception that $\mathbf{K} = \mathbf{0}$ activity exists at high levels only in generalized seizures. On the contrary, the majority of normal activity is concentrated at the lowest $\mathbf{K}$ (Nunez and Srinivasan 2006; Robinson et al. 2000; O'Connor et al. 2002; O'Connor and Robinson 2003).

The transfer functions T_{an} are written down in Appendix A for the system shown in Fig. 1. EEG spectral power is usually dominated by very low frequencies, particularly near saddle-node bifurcations, which are where voltage variances are largest (Robinson et al. 1997; Steyn-Ross et al. 1999, 2006) and which are of particular interest below. This enables the T_{an} to be approximated and allows (13) to be analytically evaluated. Details of these steps are found in Appendix B.

Our final, closed equation set is (1)–(6), (8), (9), and

$$\sigma_{Va}^2 \approx \frac{U_n^2 E_a^2}{2A_0|A_1|}, \tag{14}$$

from (70), with the E_a and A_j defined in Appendix B. The physiological parameters that determine the quantities in (14) are not precisely known for all the corticothalamic structures of interest (see Sect. 3.1); however, previously published estimates of these parameters (Robinson et al. 2004; Rowe et al. 2004) imply that σ_{Va} is typically of the same order as the input standard deviation σ_{Vn} because typical net gains are of order unity (Robinson et al. 1997, 2001, 2004). We can estimate this quantity by noting that it is of order $1/\rho_a(V_a)$ times the standard deviation of the corresponding firing rate. If firing rates are approximately Poisson processes, the latter quantity is the square root of the typical mean firing rate of $\sim$10 s^{-1} (Robinson et al. 2004), giving a standard deviation of $\sim$3 s^{-1}. This implies $\sigma_{V_a} \sim 1$ mV $\approx 0.3\sigma_\theta$ under typical conditions. Alternatively, estimates from scalp EEG signals (a few μV) also yield $\sigma_{Va} \sim 1$ mV after allowing for attenuation by a factor of $\sim$100 by volume conduction (Nunez 1995; Nunez and Srinivasan 2006). These estimates imply that σ_{V_a} is usually small enough that there are regimes where the constant-variance approximation is reasonable (thus explaining its many successful applications, as mentioned in Sect. 1), while it is large enough that other regimes exist where variance feedback will be significant (e.g., near instability and/or at high levels of external stimulation).

3 Corticothalamic systems

To explore the effects of including voltage variance in the equations for the steady states and dynamics, we begin by examining the cortical part of the system shown in Fig. 1, and assume that the fields of outgoing pulses from a given population have the same propagation characteristics, regardless of their destination—a good approximation in the cortex. This enables us to write $r_{ab} = r_b$, $v_{ab} = v_b$, and thus $\gamma_{ab} = \gamma_b$ and $\phi_{ab} = \phi_b$ for $a = e, i$ and $b = e, i, s$. For simplicity, we further assume that connectivity in the cortex is random (i.e., the numbers of synapses made are proportional to the numbers of afferent and efferent neurons available, which is a good approximation (Braitenberg and Schüz 1998; Wright and Liley 1996; Robinson et al. 1997), and that the parameters $Q_{a\max}$, θ_a, and $\sigma_{\theta a}$ are the same for all populations, and write them as $Q_{\max}$, θ, and σ_θ from now on. These approximations can be easily relaxed, but at the cost of complicating the analysis and obscuring the main effects of voltage variance that we wish to explore here. In the same vein, we concentrate mostly on the cortical system to illustrate the main effects, but more general results for the system of Fig. 1 are stated in the Appendixes and discussed qualitatively in Sect. 3.5.

3.1 Cortical steady state equations

Upon making the above assumptions, and setting space and time derivatives to zero in (3) and (6), we find the equations for uniform steady states of activity

$$V_e = V_i, \tag{15}$$

$$= (v_{ee} + v_{ei}) Q_{\max} S(V_e; \sigma_e) + P_{es}, \tag{16}$$

$$P_{es} = v_{es}\phi_s = v_{es} v_{sn} \rho_s \rho_n V_n, \tag{17}$$

where V_n is the constant spatially uniform part of the external drive. If one treats σ_e as being fixed, (16) is equivalent to results in the works cited in Sect. 1. Equation (16) can be rewritten in terms of Q_e as $f(Q_e) = 0$, with

$$f(Q_e) = S^{-1}(Q_e; \sigma_e) - \nu Q_e - P_{es}, \tag{18}$$

with $\nu = \nu_{ee} + \nu_{ei}$ and where S^{-1} is the inverse of S. Using the form (9), this yields

$$f(Q_e) = \theta_e + \frac{\sigma_e}{C} \ln\left(\frac{Q_e}{Q_{\max} - Q_e}\right) - \nu Q_e - P_{es}, \tag{19}$$

whose zeros determine the global, spatially uniform fixed points of the system. These steps restrict the analysis to regions close to the fixed points of the original $\lambda = 0$ system.

We now allow for the effects of a steady-state level of fluctuations around the fixed point, and their feedback on it via their variance. In the presence of temporal fluctuations in V_n at $\mathbf{K} = \mathbf{0}$, we find

$$\sigma_e^2 = \sigma_\theta^2 + \sigma_{Ve}^2, \tag{20}$$

$$\approx \sigma_\theta^2 + \frac{U_n^2 E_e^2}{2A_0|A_1|}, \tag{21}$$

$$= \sigma_\theta^2 + \frac{\lambda}{1 - \rho_e \nu}, \tag{22}$$

$$\lambda \approx \frac{U_n^2 \rho_s^2 \nu_{es}^2}{4\left(\frac{1}{\alpha} + \frac{\nu_{ee}}{\gamma_e \nu}\right)}, \tag{23}$$

$$\rho_e = \frac{C Q_{\max}}{\sigma_e} \frac{1}{1 + \exp[-C(V_e - \theta)/\sigma_e]}, \tag{24}$$

$$= (C Q_e/\sigma_e)(1 - Q_e/Q_{\max}), \tag{25}$$

where $\rho_e = \partial Q_e/\partial V_e$ is evaluated at the steady-state value of V_e, $\rho_e \approx 1/\nu$ for small A_0 where σ_{Ve}^2 will be appreciable, and the approximation (22) holds where the second term on the right is small and positive, and on stable branches close to saddle-node bifurcations. As mentioned at the end of Sect. 2.3, estimates of the above physiological quantities (Robinson et al. 2004; Robinson 2005; Rowe et al. 2004) imply that the second term on the right of (22) can be of order unity, and thus that the fluctuation-induced changes in the effective threshold variance can be comparable with the static variance.

3.2 Cortical steady states and stability

Equation (22) yields a cubic equation in σ_e:

$$0 = (\sigma_e^2 - \sigma_\theta^2)[\sigma_e - \nu C Q_e(1 - Q_e/Q_{\max})] - \lambda \sigma_e, \tag{26}$$

which must be satisfied at the zeros of (19), where

$$\sigma_e = \frac{C(\nu Q_e + P_{es} - \theta)}{\ln[Q_e/(Q_{\max} - Q_e)]}. \tag{27}$$

If we substitute (27) into (26) and make the definitions $q = Q_e/Q_{\max}$, $\Lambda = \lambda/\sigma_{\theta e}^2$, $N = \nu C Q_{\max}/\sigma_{\theta e}$, and $U = C(P_{es} - \theta)/\sigma_{\theta e}$, where all quantities are steady-state values, we obtain a single equation whose zeros yield the fixed points of the system:

$$\begin{aligned} 0 = {} & [\{\ln[q/(1-q)]\}^2 - (Nq + U)^2] \\ & \times \{Nq + U - Nq(1-q)\ln[q/(1-q)]\} \\ & + \Lambda(Nq + U)\{\ln[q/(1-q)]\}^2. \end{aligned} \tag{28}$$

This equation has just three parameters—N, U, and Λ—the last of which represents the feedback of variance on the sigmoid.

3.3 Cortex without variance feedback ($\Lambda = 0$)

If we rearrange (28) into the form

$$\begin{aligned} 0 = {} & \ln[q/(1-q)] - (Nq + U) \\ & + \frac{\Lambda(Nq + U)\{\ln[q/(1-q)]\}^2}{h(q)}, \end{aligned} \tag{29}$$

$$\begin{aligned} h(q) = {} & \{\ln[q/(1-q)] + Nq + U\} \\ & \times \{Nq + U - Nq(1-q)\ln[q/(1-q)]\}, \end{aligned} \tag{30}$$

the zeros of the first line of (29) yield the fixed points in the absence of variance feedback on the sigmoid ($\Lambda = 0$). In this case, our previous analysis (Robinson et al. 1997, 1998, 2004) shows that either 1 or 3 roots exist, with the single root being stable in the first case, and two stable roots separated by an unstable root in the second case. In both cases, it is possible for a low-Q_e stable root to exist for physiologically realistic parameters, and we previously identified this with the normal waking state, which has nonzero firing rate even for $P_{es} = 0$ (Robinson et al. 1997, 1998). Figure 2 shows the roots as a function of the external drive parameter U for $N = 50$. At large negative U there is a single stable fixed point at low q, while a single stable high-q fixed point exists at large positive U. At intermediate U three fixed points exist—the two stable fixed points just mentioned, and an unstable one at intermediate q. All these features are in accord with those previously found and verified in the case of $\Lambda = 0$ (Robinson et al. 1997). We discuss dynamics near fixed points further near the end of this section.

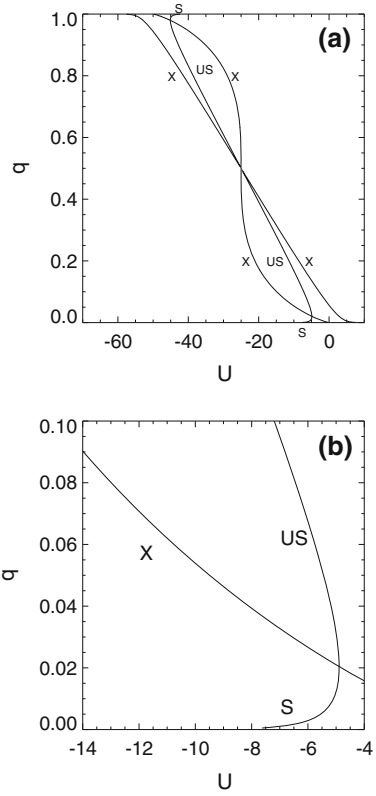

Fig. 2 Roots of the steady-state equation (28) for $\Lambda = 0$ as functions of the drive parameter U. **a** *Solid curves* show zeros of (28), with 'S' and 'US' denoting the stable and unstable branches, respectively; the two curves marked 'X' denote additional zeros of $h(q)$. **b** Zoom of part of **a**, showing the S, US, and X branches near a saddle-node bifurcation, where they all meet

As U increases in Fig. 2, the lower and middle fixed points eventually merge at a saddle-node bifurcation (Robinson et al. 1997). Near this point, provided N is large, we find $Nq \approx 1$ and $q \approx \exp(U + 1)$ at the bifurcation. Expanding $f(Q)$ to second order in Q about the bifurcation point, we find (noting that $\sigma_e = \sigma_\theta$ for $\Lambda = 0$)

$$V_e \approx \theta + (\sigma_\theta/C) \ln(\sigma_\theta/C\nu Q_{\max}) - \sqrt{2\sigma_\theta|\Delta P_{es}|/C}, \tag{31}$$

$$Q_e = \phi_e \approx (\sigma_\theta/C\nu) \exp[\pm\sqrt{2C|\Delta P_{es}|/\sigma_\theta}], \tag{32}$$

$$= \frac{\sigma_\theta}{C\nu} \pm \left(\frac{2|\Delta P_{es}|\sigma_\theta}{C\nu^2}\right)^{1/2}, \tag{33}$$

where $\Delta P_{es} = P_{es} - P_{es}^{crit}$ is the deviation (a negative quantity) from the voltage P_{es}^{crit} at the bifurcation point, the upper and lower signs refer to the unstable and lower stable branches in Fig. 2, respectively, and (33) applies for small ΔP_{es}. The trend given by (32) is for ϕ_e to increase as σ_θ increases.

If we substitute (31) and (32) into (22), we find that the voltage variance is of the form

$$\sigma_{Ve}^2 = \frac{\lambda}{1 - \exp[-\sqrt{2C|\Delta P_{es}|/\sigma_\theta}]}, \tag{34}$$

which yields

$$\sigma_{Ve}^2 \approx \lambda\sqrt{\sigma_\theta/2C|\Delta P_{es}|}, \tag{35}$$

provided $|\Delta P_{es}| \lesssim \sigma_\theta/2$; this inequality, together with the requirement $\sigma_{Ve}^2 \ll \sigma_\theta^2$ implies $\lambda \ll \sigma_\theta^2$ for the validity of (35). When this inequality is violated, one has

$$\sigma_{Ve}^2 \approx \lambda, \tag{36}$$

and justification of the approximation $\Lambda = 0$ again requires $\lambda \ll \sigma_\theta^2$ [which is equivalent to $\Lambda \ll 1$, as one might expect from direct expansion of (28)]. The above conditions imply that the small-λ approximation is valid provided $\lambda \ll \sigma_\theta^2$; i.e., provided that fluctuations do not move the system very far along the sigmoid in (9) compared to the parameter σ_θ, which is the characteristic distance over which its curvature becomes significant. The divergence of (35) as $\Delta P_{es} \to 0$ has been previously noted (Robinson et al. 1997; Steyn-Ross et al. 1999, 2006), but without derivation of prefactors from physiology.

Slow dynamics in the vicinity of fixed points can be studied by retaining only first-order time derivatives in (6) and assuming $\omega \ll \alpha, \beta, \gamma_e$, and this also allows us to determine the low-frequency stability of these points very easily via a force function or, equivalently, a potential function (Robinson et al. 1998). It is straightforward to show that the resulting dynamical equation for the corticothalamic system must have the form

$$\frac{d\phi_e(t)}{dt} = \frac{\gamma_e}{2} g[\phi_e(t), \phi_e(t - t_0), \phi_n(t - t_0/2)], \tag{37}$$

for equal corticothalamic and thalamocortical delays, where g is a function whose form is determined by solving a transcendental equation (Kim and Robinson 2007). This form is equivalent to that of friction-dominated dynamics of a particle under the influence of a force g. If the cortex alone is considered, one can simply set $t_0 = 0$ in (36) and omit the redundant second copy of the repeated argument $\phi_e(t)$ on the right to give a simplified two-argument function. In Appendix C we derive the equivalent form by a route more similar to that used in earlier work (Robinson et al. 1998). This yields

$$\frac{d\phi_e(t)}{dt} \approx \frac{\gamma_e}{2} \frac{F[\phi_e(t)]}{|\nu_{ei}| + 1/\rho_e}, \tag{38}$$

with $F[\phi_e(t)]$ given by (77)–(80), which generalize previous results (Robinson et al. 1998) to include variance feedback. The force function F has zeros at the fixed points of the system dynamics, whose locations are modified via the dependences on the σ_a, and the effective inertia [proportional to the denominator in (37)] also increases with increasing σ_e. Applied to Fig. 2, the force function confirms that the upper right and lower left branches are stable, with dynamics causing the system to approach the fixed point.

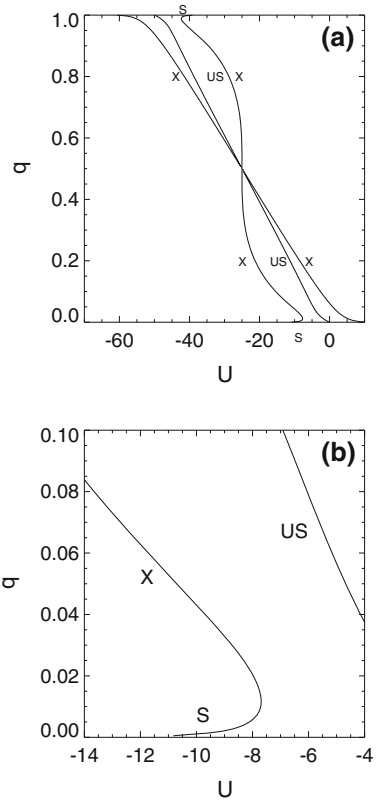

Fig. 3 Roots of the steady-state equation (28) for $\Lambda = 1$ as functions of the drive parameter U. **a** *Solid curves* show zeros of (28), as in Fig. 2. **b** Zoom of part of **a**, showing the stable (S), unstable (US), and X branches near a saddle-node bifurcation, where the X and S branches join

3.4 Cortex with variance feedback ($\Lambda \neq 0$)

If we set $\Lambda \neq 0$ in (28) or (29), we include variance feedback in determining the steady states. Figure 3 shows the resulting fixed points for $\Lambda = 1$ (we choose this relatively large illustrative value of Λ for clarity). We see that the fixed point topology is changed, with the X branch joining smoothly onto the stable and unstable branches, instead of crossing. The result is that the bifurcation point is moved to lower U than in Fig. 2, implying that the system is less stable, which can be understood qualitatively by noting that this fixed point has $V_e < \theta_e$, so an increase in σ_e in (9) pushes the system to higher firing rates for given inputs, and thus closer to instability. Accordingly, the firing rate at the bifurcation point is lower for nonzero Λ.

The behavior of the lower stable branch (corresponding to normal brain activity) in Fig. 2 can be understood analytically by substituting (35) into (8) and expanding to first order in λ. If $|\Delta P_{es}| \lesssim \sigma_\theta/2$, then

$$\sigma_e \approx \sigma_\theta + \lambda/(8C\sigma_\theta|\Delta P_{es}|)^{1/2}; \tag{39}$$

otherwise, $\sigma_e \approx \sigma_\theta + \lambda/2\sigma_\theta$. By expanding (32) around the saddle node bifurcation (where $\Delta P_{es} = 0$), (38) can be re-expressed as

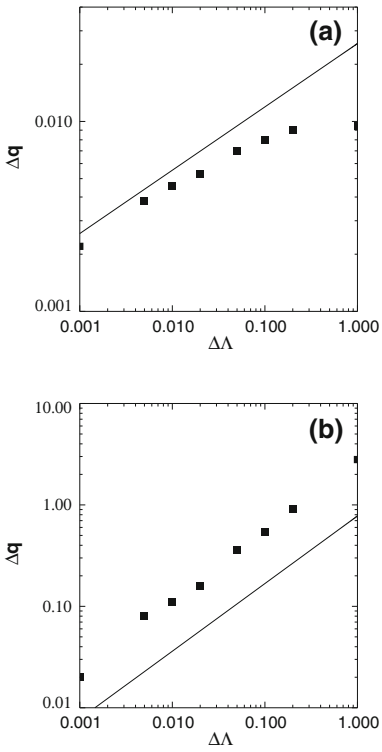

Fig. 4 Scalings of bifurcation point versus Λ. **a** $|\Delta q|$, with the *solid line* showing the prediction (41). **b** $|\Delta U|$, with the *solid line* showing the prediction (42)

$$\sigma_e \approx \sigma_\theta + \frac{\lambda}{2C\nu(Q_0 - Q)}, \tag{40}$$

for $Q < Q_0$ where Q_0 is the location of the bifurcation point for $\Lambda = 0$.

If we again expand $f(Q_e)$ to second order in Q relative to the saddle-node bifurcation, assuming small Q_e, but using (39) for σ_a, we find that the firing rate on the curve at given ΔP_{es} is changed relative to the $\lambda = 0$ case (32) by an amount

$$\Delta Q = -Q_0 \left[\frac{\Lambda}{2} \ln\left(\frac{1}{q_0}\right) \right]^{1/3}, \tag{41}$$

with $q_0 = \sigma_\theta / C\nu Q_{\max} \approx 1/N$ [see just before Eq. (31)] and $Q_0 = Q_{\max} q_0$, provided the right hand side remains small compared to Q_0 (higher order corrections are, of course, required close to the bifurcation). Numerical calculation of the location of the rightmost point on the lower stable branch (seen in Figs. 2, 3) confirms the form (41), with reasonable quantitative agreement for $\Lambda \lesssim 0.1$, as shown in Fig. 4a.

By re-expressing ΔP_{es} in terms of ΔQ, via (33), we find that the shift in the bifurcation point relative to its location at $\Lambda = 0$ is

$$\Delta U \approx -\frac{1}{2} \left[\frac{\Lambda}{2} \ln\left(\frac{1}{q_0}\right) \right]^{2/3}, \tag{42}$$

since $\Delta U = C\Delta P_{es}/\sigma_\theta$. The $\Lambda^{2/3}$ scaling of this result agrees with numerical results, as seen in Fig. 4b, but the numerical normalization is found to be roughly twice as large, apparently due to the change in topology of the modes for $\Lambda > 0$.

The noninteger scalings in (41) and (42) do not appear to have been previously noted in the literature. Since their derivatives with respect to Λ diverge at $\Lambda = 0$, they imply that the bifurcation point is extremely sensitive to variance feedback, even for small values of Λ (although the range over which this sensitivity is significant shrinks as Λ decreases). From (23) we see that Λ is a quadratic function of stimulus amplitude, so strong stimuli favor Λ-dependent effects.

3.5 Corticothalamic case

In the full corticothalamic system of Fig. 1, there are both excitatory and inhibitory feedbacks of the cortex on itself via the thalamus, which itself contains distinct excitatory and inhibitory structures. These effects can change the position of the saddle-node bifurcation relative to the purely cortical case (Robinson et al. 1998, 2002, 2004), where this position is determined by the zero of the denominator $1 - \rho_e \nu$ in (22), and this denominator is proportional to A_0 [see (70)]. In the corticothalamic case, the more general result (68) must be used for A_0, so the corresponding denominator is

$$1 - \rho_e(\nu + \rho_s \nu_{es}\nu_{se} + \rho_s\rho_r \nu_{es}\nu_{sr}\nu_{re}), \tag{43}$$

whose zero determines the location of the saddle-node bifurcation and the associated spectral divergence.

Since only ν_{sr} is negative in (43), the net effect of the additional terms in this expression can be positive or negative. The overall effects of including voltage variance can be to increase or decrease the proximity to the saddle-node bifurcation, increase or decrease firing rates, and/or destabilize or stabilize the system relative to the case with $\Lambda = 0$. Using the results (40) and (41), and expanding in powers of $\Lambda^{1/3}$, we can write

$$\rho_a = \rho_a^{(0)} + \rho_a^{(1)}\Lambda^{1/3}, \tag{44}$$

to lowest nontrivial order, where $\rho_a^{(0)}$ and $\rho_a^{(1)}$ are constants. On substituting (44) into (43), the sign of the Λ-dependent terms proves to be a nonlinear function of the system state, which cannot be expressed in closed form because it involves the solution of a set of transcendental equations for the steady states (Robinson et al. 1998, 2002, 2004). Moreover, the bifurcation structure near the instability onset has a resulting complex dependence on multiple parameters (Breakspear et al. 2006). Hence, numerical analysis, based in part on the expressions derived here, will be needed to obtain systematic results. Nonetheless, the example in the next paragraph gives some insight into the effects to be expected.

In an exemplar case with $G_{rs} = 0$ (which simplifies the situation by severing the intrathalamic feedback loop in Fig. 1), (68) can be interpreted as involving both direct cortical feedback on itself, embodied in the gains $G_{ee} = \rho_e \nu_{ee}$ and $G_{ei} = \rho_e \nu_{ei}$, and feedbacks via the thalamus, embodied in the other gains. In the waking state, the positive term $\rho_s \nu_{es} \nu_{se}$ is larger than the final term in (43) and steady state firing rates in cortex and thalamus increase in tandem with increasing external drive (Robinson et al. 2001, 2002, 2004). This causes ρ_e and ρ_s to increase with increasing Λ, leading to earlier onset of the saddle-node bifurcation. In sleep, the negative term $\rho_s \rho_r \nu_{es} \nu_{sr} \nu_{re}$ is the larger of the final two terms in (43), and the reticular nucleus has an elevated firing rate, while the relay nuclei's activity is suppressed (Robinson et al. 2001, 2004). This leads to the Λ dependence of the final term in (43) opposite to that of the remainder of the expression, thus tending to postpone the onset of the saddle-node bifurcation, which may help to oppose the onset of some types of epileptic seizure (Robinson et al. 2002; Breakspear et al. 2006).

4 Summary and discussion

We have extended a widely applied neural field theory to approximate the effects of feedback of voltage variance on the firing-rate response function. In particular, we have examined how voltage fluctuations feed back on the nonlinear response properties of neural field models to affect the fixed points that correspond to steady states, perturbing them away from their no-feedback forms. This has been done by calculating the contribution of these fluctuations to the standard deviation of the threshold of the rate-voltage response function, using linear theory to approximate the variance. The regimes of validity of approaches with and without variance feedback have been estimated. Results found for adiabatic dynamics enable the system evolution to be tracked in the vicinity of the fixed points in the presence of variance feedback.

It has been found that the likely magnitude of variance-feedback effects is small in many situations, thereby explaining the widespread success of constant-variance theories in explaining many EEG phenomena. However, the variance coupling strength can be sufficiently large to cause significant effects, especially near saddle-node bifurcations of brain dynamics where the brain is close to a marginal stability, a state that its dynamics are widely believed to favor.

The main effects of variance feedback are found to occur near saddle-node bifurcations, where the low-frequency spectral power diverges. The divergence of the voltage variance scales with the same exponent of $1/2$ as estimated in previous work, but the normalization is calculated here from physiology for the first time. Noninteger exponents of $2/3$ and $1/3$ are found for the scaling versus variance coupling strength Λ of the position and firing rate, respectively, at the saddle-node bifurcation of the stable branch corresponding to normal brain activity. Significantly, these noninteger exponents imply a high susceptibility of the steady state properties to variance feedback. Since the brain is thought to operate relatively close to the saddle-node bifurcation to maintain marginal stability (Robinson et al. 1997, 2001, 2004), the resulting modulations may be significant in normal brain states, especially if external stimuli are strong, since Λ increases in proportion to the power input from external stimuli. This

may also provide a route to probe and manipulate such effects experimentally, and thus to estimate quantities such as Λ, σ_e, and their underlying physiological variables in vivo.

For a cortical system, it is found that fixed points tend to be destabilized by variance feedback, but in the full corticothalamic system, they can either be destabilized or stabilized, depending on the sign of the thalamic feedback and the precise state of the system. Full analysis of the effects of variance dynamics on these characteristics and on seizure onset will require inclusion of effects on the Hopf bifurcations that lead most directly to seizure onset at higher frequencies (Robinson et al. 2002; Breakspear et al. 2006). Another possible outcome of the differential effects of variance dynamics on the components of the corticothalamic system is that they may introduce additional fixed points by modifying the gains into regions where at least five fixed points are already known to be possible (Robinson et al. 1998, 2004). This could affect some of the phase transitions that have been argued to be related to sleep and anesthesia (Steyn-Ross et al. 1999, 2001a,b, 2005a, 2006). Further applications of the present results would include extension to include higher moments, and detailed investigation of steady states, bifurcation structures, and seizure thresholds in the full corticothalamic system. Contributions of axonal voltage fluctuations via antidromic propagation to the cell body and dendritic synapses could also be included.

Acknowledgments The author thanks A. N. Burkitt, A. Peterson, H. Meffin, and D. B. Grayden for stimulating discussions. The Australian Research Council supported this work.

Appendix A: Transfer functions

Transfer functions for the systems shown in Fig. 1 have been derived before, mainly in the form required to express ϕ_a in terms of ϕ_n (Robinson 2005). These can be straightforwardly re-expressed in the form linking V_a to V_n required here; i.e., $T_{an} = V_a(\mathbf{k}, \omega)/V_n(\mathbf{k}, \omega)$.

For the corticothalamic system in Fig. 1, at $\mathbf{k} = \mathbf{0}$, and assuming the simplifications mentioned in Sect. 2.3 and at the start of Sect. 3, we find

$$T_{en} = \frac{\rho_n D_e}{\rho_e} \frac{\phi_e}{\phi_n}, \tag{45}$$

$$\frac{\phi_e}{\phi_n} = \frac{J_{es} J_{sn}}{(1 - J_{sr} J_{rs})(1 - J_{ei})} \frac{1}{q^2 r_e^2}, \tag{46}$$

$$D_e = (1 - i\omega/\gamma_e)^2, \tag{47}$$

$$q^2 r_e^2 = D_e - \frac{1}{1 - J_{ei}} \left[J_{ee} + \frac{J_{es}(J_{se} + J_{sr} J_{re})}{1 - J_{sr} J_{rs}} \right], \tag{48}$$

$$J_{ab} = L_{ab}(\omega) G_{ab} e^{i\omega\tau_{ab}}, \tag{49}$$

$$L_{ab} = (1 - i\omega/\alpha_{ab})^{-1} (1 - i\omega/\beta_{ab})^{-1}, \tag{50}$$

$$G_{ab} = \rho_a \nu_{ab}, \tag{51}$$

where the parameters in (45)–(51) are defined in Sect. 2.1. In deriving (45)–(51) we have noted that for the parameters of relevance here, $D_i \approx D_r \approx D_s \approx 1$ (Robinson 2005). Henceforth, we also set $\alpha_{ab} = \alpha$ and $\beta_{ab} = \beta$ for all ab for simplicity, and we set all the $\tau_{ab} = 0$ except for $\tau_{se} = \tau_{re} = \tau_{es} = t_0/2$, where t_0 is a constant (Robinson 2005).

Likewise, one finds

$$T_{in} = T_{en}, \tag{52}$$

$$T_{sn} = \frac{\rho_n}{\rho_s(1 - J_{sr}J_{rs})}\left[(J_{se} + J_{sr}J_{re})\frac{\phi_e}{\phi_n} + J_{sn}\right], \tag{53}$$

$$T_{rn} = \frac{\rho_n}{\rho_r(1 - J_{sr}J_{rs})}\left[(J_{re} + J_{rs}J_{se})\frac{\phi_e}{\phi_n} + J_{rs}J_{sn}\right]. \tag{54}$$

The case of a cortical system is derived from Fig. 1 by setting $J_{re} = J_{se} = J_{rs} = J_{sr} = 0$, so (45)–(54) yield

$$T_{en} = \frac{\rho_n D_e J_{es} J_{sn}}{\rho_e(1 - J_{ei})}\frac{1}{q^2 r_e^2}, \tag{55}$$

$$q^2 r_e^2 = D_e - \frac{J_{ee}}{1 - J_{ei}}, \tag{56}$$

with (52) continuing to apply.

Appendix B: Approximate evaluation of transfer functions

The transfer functions (and spectrum) in (13) are often dominated by low frequencies. This is especially true near a saddle-node bifurcation, when the global steady state loses stability at zero frequency (Robinson et al. 1997). Hence, we seek to approximate the T_{an} at small ω. We note that the transfer functions in Appendix A can all be written as

$$T_{an}(\omega) \approx \frac{E_a}{q^2(\omega)r_e^2} + F_a(\omega), \tag{57}$$

where the E_a are constants, with

$$E_e = \frac{\rho_n}{\rho_e}\frac{G_{es}G_{sn}}{(1 - G_{sr}G_{rs})(1 - G_{ei})}, \tag{58}$$

$$E_i = E_e, \tag{59}$$

$$E_s = \frac{\rho_e}{\rho_s}\frac{J_{se} + J_{sr}J_{re}}{1 - G_{sr}G_{rs}}E_e, \tag{60}$$

$$E_r = \frac{\rho_e}{\rho_r}\frac{J_{re} + J_{rs}J_{se}}{1 - G_{sr}G_{rs}}E_e, \tag{61}$$

for the system of Fig. 1, and

$$E_e = \frac{\rho_n G_{es} G_{sn}}{\rho_e (1 - G_{ei})}, \tag{62}$$

for the cortical system derived from Fig. 1, with (59) also applying. Here the random connectivity approximation has been invoked to infer that $\rho_e = \rho_i$ in deriving (58)–(62).

The cases in which σ_{Va} affects the dynamics significantly are those where it is large. These correspond to $q^2 r_e^2$ being close to zero at $\omega = 0$. We thus expand $q^2(\omega)$ to second order in $-i\omega$, writing

$$q^2(\omega) r_e^2 \approx A_0 - i\omega A_1 - \omega^2 A_2, \tag{63}$$

where the coefficients A_j are discussed below and this equation is valid provided ω is small compared to α, β, γ_e, and $2\pi/t_0$, which are all of order 100 s^{-1} (Robinson et al. 2004; Robinson 2005).

Sufficiently close to the zero of $q^2(\omega)$ we can consider only the first term in (57). Then (13) becomes

$$\sigma_{Va}^2 \approx U_n^2 \int \frac{d\omega}{2\pi} \frac{|E_a|^2}{|A_0 - i\omega A_1 - \omega^2 A_2|^2}, \tag{64}$$

$$\approx U_n^2 \int \frac{d\omega}{2\pi} \frac{E_a^2}{A_0^2 + (A_1^2 - 2A_0 A_2)\omega^2}, \tag{65}$$

$$= \frac{U_n^2 E_a^2}{2A_0 \sqrt{A_1^2 - 2A_0 A_2}}, \tag{66}$$

where terms of order ω^3 and higher have been neglected in obtaining (65) from (64) and $A_0 > 0$ is required for the state to be stable at zero frequency (Robinson et al. 1997, 2001). Equation (66) usually only yields large contributions for cases where the denominator is small. In particular, $A_0 = 0$ represents a saddle-node bifurcation where the spectrum diverges (Robinson et al. 1997, 2001, 2002; Steyn-Ross et al. 1999, 2006). In this vicinity, we can make the further approximation

$$\sigma_{Va}^2 \approx \frac{U_n^2 E_a^2}{2A_0 |A_1|}, \tag{67}$$

provided A_1 is nonzero.

The coefficients A_0 and A_1 in (63) are given by

$$A_0 = \frac{1}{1-G_{ei}}\left[1 - G_{ee} - G_{ei} - \frac{G_{es}(G_{se}+G_{sr}G_{re})}{1-G_{sr}G_{rs}}\right], \tag{68}$$

$$A_1 = \frac{2}{\gamma_e} + \frac{1}{1-G_{ei}}\left(\frac{1}{\alpha}+\frac{1}{\beta}\right)\left[1 - A_0 + \frac{G_{es}}{1-G_{sr}G_{rs}}\left\{(G_{se}+G_{sr}G_{re}) \times \left(\frac{\alpha\beta t_0}{\alpha+\beta} + \frac{2}{1-G_{sr}G_{rs}}\right) - G_{se}\right\}\right], \tag{69}$$

for the system in Fig. 1, which yields

$$A_0 = 1 - \frac{G_{ee}}{1-G_{ei}}, \tag{70}$$

$$A_1 = \frac{2}{\gamma_e} + \left(\frac{1}{\alpha}+\frac{1}{\beta}\right)\frac{G_{ee}}{(1-G_{ei})^2}, \tag{71}$$

for the cortical system of Fig. 1.

Appendix C: Adiabatic dynamics

Here we derive equations for the adiabatic dynamics of the system near to fixed points, in terms of a force function that can be integrated to obtain a potential.

If we set the α_{ab} and β_{ab} to infinity in (3) and assume that the τ_{ab} are short compared to the time scales of the slow dynamics. If we retain only the first-order time derivative in (6) and ignore spatial structure for now, as in the rest of the paper, we find (using the random connectivity approximation)

$$\left(\frac{2}{\gamma_e}\frac{d}{dt} + 1\right)\phi_e = S(V_e;\sigma_e), \tag{72}$$

$$\phi_i = S(V_e;\sigma_e), \tag{73}$$

$$\phi_s = S(V_s;\sigma_s), \tag{74}$$

$$\phi_r = S(V_e;\sigma_r). \tag{75}$$

From these equations, one can eliminate ϕ_i, ϕ_s, and ϕ_r in turn. This yields steady-state equations equivalent to those of Robinson et al. (2004) if variances are fixed and equal. More generally, expansion of terms involving $D_e\phi_e$ in Taylor series in d/dt yields

$$\frac{d\phi_e(t)}{dt} \approx \frac{\gamma_e}{2}\frac{F[\phi_e(t)]}{|v_{ei}| + (1-G_{sr}G_{rs})/\rho_e}, \tag{76}$$

with

$$F[\phi_e(t)] = S^{-1}[\phi_e(t);\sigma_e] - (\nu_{ee}+\nu_{ei})\phi_e(t) - \nu_{es}S[V_s(t);\sigma_s], \quad (77)$$

$$V_s(t) = \nu_{se}\phi_e(t) + \nu_{sn}\phi_n(t) + \nu_{sr}S[V_r(t);\sigma_r], \quad (78)$$

$$V_r(t) = \nu_{re}\phi_e(t) + (\nu_{rs}/\nu_{es})S^{-1}[\phi_e(t);\sigma_e], \quad (79)$$

$$S^{-1}(\phi_a;\sigma_a) = \theta_a + (\sigma_a/C)\ln[q_a/(1-q_a)], \quad (80)$$

with the σ_a obeying (8) and (67).

The purely cortical case is obtained from (76)–(80) by setting $G_{rs}G_{rs} = 0$ in (76) and $\nu_{se} = \nu_{sr} = \nu_{rs} = \nu_{sr} = 0$ in (77)–(79).

References

Bojak I, Liley DTJ (2005) Modeling the effects of anesthesia on the electroencephalogram. J Clin Neurophysiol 22:300

Braitenberg V, Schüz A (1998) Cortex: statistics and geometry of neuronal connectivity, 2nd edn. Springer, Berlin

Breakspear M, Roberts JA, Terry JR, Rodrigues S, Mahant N, Robinson PA (2006) A unifying explanation of primary generalized seizures through nonlinear brain modeling and bifurcation analysis. Cereb Cortex 16:1296

Bressloff PC (2002) Bloch waves, periodic feature maps, and cortical pattern formation. Phys Rev Lett 59:088101

Bressloff PC (2009) Stochastic neural field theory and the system-size expansion. SIAM J Appl Math 70:1488

Bressloff PC, Cowan JD (2002) SO (3) symmetry breaking mechanism for orientation and spatial frequency tuning in the visual cortex. Phys Rev Lett 88:078102

Buice MA, Cowan JD (2007) Field-theoretic approach to fluctuation effects in neural networks. Phys Rev E 75:051909

Buice MA, Cowan JD (2009) Statistical mechanics of the neocortex. Prog Biophys Molec Biol 99:53

Buice MA, Cowan JD, Chow CC (2010) Systematic fluctuation expansion for neural network activity equations. Neural Comput 22:377

Deco G, Jirsa VK, Robinson PA, Breakspear M, Friston K (2008) The dynamic brain: from spiking neurons to neural masses and cortical fields. Publ Lib Sci Comp Biol 4:e1000092

Freeman WJ (1975) Mass action in the nervous system. Academic, New York

Jirsa VK, Haken H (1996) Field theory of electromagnetic brain activity. Phys Rev Lett 77:960–963

Kim JW, Robinson PA (2007) Compact dynamical model of brain activity. Phys Rev E 75:031907

Lopes da Silva FH, Hoeks A, Smits H, Zetterberg LH (1974) Model of brain rhythmic activity the alpha-rhythm of the thalamus. Kybernetik 15:27–37

Marreiros AC, Daunizeau J, Kiebel SJ, Friston KJ (2008) Population dynamics: variance and the sigmoidal activation function. Neuroimage 42:147

Marreiros AC, Kiebel SJ, Friston KJ (2010) A dynamic causal model study of neuronal population dynamics. Neuroimage 51:91

Meffin H, Burkitt AN, Grayden DB (2004) An analytical model for the 'large, fluctuating synaptic conductance state' typical of neocortical neurons in vivo. J Comp Neurosci 16:159–175 and references cited therein

Nunez PL (1974) Wavelike properties of the alpha rhythm. IEEE Trans Biomed Eng 21:473–482

Nunez PL (1995) Neocortical dynamics and human EEG rhythms. Oxford University Press, Oxford

Nunez PL, Srinivasan R (2006) Electric fields of the brain. Oxford University Press, Oxford

O'Connor SC, Robinson PA (2003) Wave-number spectrum of electrocorticographic signals. Phys Rev E 67:051912

O'Connor SC, Robinson PA, Chiang AKI (2002) Wave-number spectrum of electroencephalographic signals. Phys Rev E 66:061905
Rennie CJ, Robinson PA, Wright JJ (2002) Unified neurophysical model of EEG spectra and evoked potentials. Biol Cybern 86:457–471
Robinson PA (2005) Propagator theory of brain dynamics. Phys Rev E 72:011904
Robinson PA, Loxley PN, O'Connor SC, Rennie CJ (2000) Modal analysis of corticothalamic dynamics, electroencephalographic spectra, and evoked potentials. Phys Rev E 63:041909
Robinson PA, Rennie CJ, Rowe DL (2002) Dynamics of large-scale brain activity in normal arousal states and epileptic seizures. Phys Rev E 65:041924
Robinson PA, Rennie CJ, Rowe DL, O'Connor SC (2004) Estimation of multiscale neurophysiologic parameters by electroencephalographic means. Hum Brain Mapp 23:53–72
Robinson PA, Rennie CJ, Wright JJ (1997) Propagation and stability of waves of electrical activity in the cerebral cortex. Phys Rev E 56:826–840
Robinson PA, Rennie CJ, Wright JJ, Bourke PD (1998) Steady states and global dynamics of electrical activity in the cerebral cortex. Phys Rev E 58:3557
Robinson PA, Rennie CJ, Wright JJ, Bahramali H, Gordon E, Rowe DL (2001) Prediction of electroencephalographic spectra from neurophysiology. Phys Rev E 63:021903
Robinson PA, Wu H, Kim JW (2007) Neural rate equations for bursting dynamics derived from conductance-based equation. J Theor Biol 250:663–672
Rowe DL, Robinson PA, Rennie CJ (2004) Estimation of neurophysiological parameters from the waking EEG using a biophysical model of brain dynamics. J Theor Biol 231:413–433
Rubino D, Robbins KA, Hatsopoulos NG (2006) Propagating waves mediate information transfer in the motor cortex. Nat Neurosci 9:1549–1557
Schiff SJ, Huang X, Wu JY (2007) Dynamical evolution of spatiotemporal patterns in mammalian middle cortex. Phys Rev Lett 98:178102
Steyn-Ross DA, Steyn-Ross ML, Sleigh JW, Wilson MT, Gillies IP, Wright JJ (2005) The sleep cycle modelled as a cortical phase transition. J Biol Phys 31:547–569
Steyn-Ross DA, Steyn-Ross ML, Wilcocks LC, Sleigh JW (2001) Toward a theory of the general-anesthetic-induced phase transition of the cerebral cortex. II. Numerical simulations, spectral entropy, and correlation times. Phys Rev E 64:011918
Steyn-Ross ML, Steyn-Ross DA, Sleigh JW, Liley DTJ (1999) Theoretical electroencephalogram stationary spectrum for a white-noise-driven cortex: Evidence for a general anesthetic-induced phase transition. Phys Rev E 60:7299
Steyn-Ross ML, Steyn-Ross DA, Sleigh JW, Wilcocks LC (2001) Toward a theory of the general-anesthetic-induced phase transition of the cerebral cortex. I. A thermodynamics analogy. Phys Rev E 64:011917
Steyn-Ross ML, Steyn-Ross DA, Sleigh JW, Wilson MT, Wilcocks LC (2005) Proposed mechanism for learning and memory erasure in a white-noise-driven sleeping cortex. Phys Rev E 72:061910
Steyn-Ross ML, Steyn-Ross DA, Sleigh JW, Wilson MT, Wilcocks LC (2005) Proposed mechanism for learning and memory erasure in a white-noise-driven sleeping cortex. Phys Rev E 72:051920
Suffczynski P, Lopes da Silva FH, Parra J, Velis D, Kalitzin S (2005) Epileptic transitions: model predictions and experimental validation. J Clin Neurophysiol 22:288
Suffczynski P, Wendling F, Bellanger JJ, Da Silva FHL (2006) Some insights into computational models of (Patho) physiological brain activity. Proc IEEE 94:784–804
Wilson HR, Cowan JD (1973) Mathematical theory of functional dynamics of cortical and thalamic nervous-tissue. Kybernetik 13:55–59
Wright JJ, Liley DTJ (1996) Dynamics of the brain at global and microscopic scales: Neural networks and the EEG. Behav Brain Sci 19:285
Xu WF, Huang XY, Takagaki , Wu JY (2007) Compression and reflection of visually evoked cortical waves. Neuron 55:119